



OPEN

## Bioinformatics and experimental insights into F2RL1 as a key biomarker in cervical cancer diagnosis and prognosis

Yonggang Dai<sup>1,2</sup>, Chunxiang Li<sup>3</sup>, Shiliang Cheng<sup>1</sup>, Hongya Wang<sup>1</sup> & Xuewei Zhuang<sup>1</sup>✉

Cervical cancer(CCa) remains a significant global public health concern, with early diagnosis and treatment being crucial. Moreover, the molecular mechanisms underlying its pathogenesis remain incompletely elucidated. F2RL1 is closely associated with various tumors. However, its relationship with CCa is poorly understood. We accessed data from 309 patients diagnosed with CCa from TCGA database. The Limma package facilitated differential expression analysis to identify differentially expressed mRNAs (DEmRNAs). Survival analysis and ROC analysis were conducted via the XIANTAO database. Immune-related genes were identified with F2RL1-related genes through ImmPort database analysis. Functional enrichment analysis was carried out using GO, KEGG, and GSEA. We gathered cervical cells and serum from participants to test for HPV and TCT, and then used qPCR to check the levels of F2RL1 mRNA expression. We also verified the expression of F2RL1 protein through WB and ELISA techniques. Our investigation has unveiled a fascinating discovery—the levels of F2RL1 expression in CCa tissues are notably elevated when compared to normal tissues, showcasing intriguing variations among various pathological types. Moreover, the presence of high F2RL1 expression is linked to reduce Overall Survival (OS), Progression Free Interval (PFI), Progression Free Survival (PFS). F2RL1 rocked the ROC analysis with an AUC of 0.996. Furthermore, F2RL1 expression levels significantly impact CCa in different N stages, pathological tissue types, treatment statuses, and racial groups, allowing us to develop a predictive model. Additionally, we identified 43 immune-related genes. Enrichment analysis highlighting their association with pathways related to cell movement and T cell activation. Through analysis, we discovered an inverse proportion between F2RL1 expression and the infiltration of most immune cells, particularly TFH and cytotoxic cells, suggesting a potential link to immune evasion in CCa. Molecular biology experiments also confirmed a significant increase in F2RL1 expression in cervical exfoliated cells and serum. Our research uncovers the predictive and early detection significance of F2RL1 in CCa and its correlation with immune infiltration for the first time. F2RL1 is strongly linked to the progression of CCa and could serve as a biomarker for the early diagnosis and prognosis of CCa patients.

**Keywords** Cervical Cancer, F2RL1, Immune Infiltration, Prognosis, Biomarker

Cervical cancer (CCa) continues to be a major global health issue, standing tall as the fourth most prevalent cancer in women across the world. In 2018 alone, the World Health Organization reported a staggering 570,000 fresh diagnoses, resulting in more than 311,000 unfortunate deaths on a global scale<sup>1</sup>. The alarming number of lives lost, especially in less affluent nations, highlights the pressing demand for enhanced methods of diagnosis and treatment<sup>2</sup>. Despite the availability of preventive vaccines and early screening methods, both the incidence and mortality rates remain high, indicating the complexity of the disease and the necessity for further research into its molecular underpinnings<sup>1</sup>. Current treatments, such as surgery, radiotherapy, and chemotherapy, often have significant side effects and are less effective in advanced stages of the disease<sup>3</sup>. These difficulties highlight

<sup>1</sup>Department of Clinical Laboratory, Shandong Provincial Third Hospital, Shandong University, No.11 Middle Wuyingshan Road, Tianqiao, Jinan 250031, Shandong, China. <sup>2</sup>College of First Clinical Medicine, Shandong University of Traditional Chinese Medicine, Jinan, Shandong, China. <sup>3</sup>Department of Clinical Microbiology Laboratory, Shandong Second Provincial General Hospital, Jinan, Shandong, China. ✉email: zhuangxuewei@sdu.edu.cn

the pressing requirement for enhanced diagnostic and treatment approaches, which rely on a more profound comprehension of the molecular foundations of CCa<sup>4</sup>.

F2R Like Trypsin Receptor 1 (F2RL1), also referred to as Proteinase-Activated Receptor 2 (PAR2), is a G-protein-coupled receptor involved in various cellular functions such as inflammation, pain sensation, and cancer advancement<sup>5</sup>. F2RL1 has been shown to modulate the tumor microenvironment, angiogenesis, and metastasis, suggesting its potential significance in cancer biology<sup>6,7</sup>. Besides thrombin, F2RL1 can be activated by various proteases, contributing to inflammatory responses and strongly linked with the establishment of the tumor microenvironment and malignancy<sup>8</sup>. Additionally, the role of tumor microenvironment in tumor metastasis has drawn increasing attention from researchers<sup>9,10</sup>. However, due to its complexity and variability, the mechanisms through which the tumor microenvironment promotes metastasis remain incompletely understood<sup>9,11,12</sup>. Serine proteases like pancreatic trypsin, thrombin, and tissue factor have the power to awaken PARs on cell surfaces, triggering a range of biological impacts that influence the emergence of inflammation and tumors<sup>13,14</sup>. Research has revealed that F2RL1 is abundantly present in a multitude of cancerous tissues and cells, including those found in esophageal, gastric, liver, and colorectal cancers<sup>15,16</sup>. Activation of this receptor triggers a cascade of biological behaviors connected with tumor growth, invasion, and metastasis<sup>14,17,18</sup>. For example, in pancreatic cancer cells, the presence and activation of F2RL1 play a key role in fueling their growth, movement, and infiltration. Conversely, in colorectal cancer, while PAR1 and F2RL1 are typically found in normal stroma, their presence is heightened in the stroma of tumor cells<sup>5,13,19–21</sup>. In gastric cancer tissues, the expression of F2RL1 is closely related to the depth of tumor invasion into the gastric wall, lymphatic and venous infiltration, and the occurrence of liver metastasis<sup>22,23</sup>. (In cervical cancer, understanding of F2RL1 expression and function remains limited, although emerging evidence suggests its potential impact on tumor progression and patient prognosis<sup>24,25</sup>.

In this research, our goal is to explore the potential of F2RL1 as both a prognostic indicator and a target for therapy in CCa<sup>24</sup>. The anticipated findings could offer fresh perspectives into the pathogenesis of the disease and contribute to the development of personalized medicine approaches for cervical cancer patients.

## Materials & methods

### RNA-seq data and bioinformatics analysis

This research made use of data obtained from the TCGA database (<https://portal.gdc.cancer.gov>). RNA-seq data from the TCGA–Cervical Squamous Cell Carcinoma (CESE) project underwent the STAR workflow and were extracted in TPM format to gather gene expression and clinical information. The dataset comprised 255 cases of squamous carcinoma, 47 cases of adenocarcinoma, 7 cases of adenosquamous tissue, and 3 cases of normal tissue. Information such as name, age, race, T-stage, N-stage, M-stage, pathologic type, and treatment status was included. Data processing and visualization were conducted using R software (v4.2.1), eliminating clinically uninformative and duplicate data. Statistical analyses were conducted using the “stats” and “car” packages in R, and visualization was accomplished using the “ggplot2” package. This study adhered to the Declaration of Helsinki (2013 revision) and followed the publication guidelines outlined by TCGA.

### Analysis of differentially expressed mRNAs (DEmRNAs)

The data in this study were normalised and log-transformed (TPM), so we used the ‘limma’ package, setting the criteria of  $|\log FC| > 1.5$  and  $P.\text{adj} < 0.05$ . Visualization was done through the creation of a volcano plot for mRNA and a heatmap displaying the target gene and its co-expressed mRNA, using the “ggplot2” package. Immunohistochemical staining data for F2RL1 were sourced from the HPA database (<http://www.proteinatlas.org/>).

### Survival and ROC analysis

For the analysis of DEmRNAs linked to CCa patient prognosis, the “Survival” package was employed. Patients were divided into high and low expression groups based on the median expression of DEmRNAs. Survival curves were generated using the Kaplan–Meier Plotter (<https://kmplot.com/>)<sup>26</sup>. Additionally, ROC analysis was performed using the “pROC” package<sup>27</sup>, utilizing data from XIANTAO (<https://www.xiantaozi.com/>).

### Identification of the target gene linked to immunity

The ImmPort database (<https://www.immport.org/shared/home>) was used to identify immune-related genes<sup>28</sup>. Venn diagram shows the connection between prognostically associated DEmRNAs and immune-related genes, leading to the identification of F2RL1 as the target gene. A PPI network and hub genes screening were conducted utilising the STRING database (<https://string-db.org/cgi/input.pl>) and the cytohubba plugin for Cytoscape (v3.10.1). The MCC algorithm was employed to identify the top 10 genes.

### Functional enrichment analysis by GO, KEGG and GSEA

To investigate the functions of F2RL1, we conducted Gene Ontology (GO), Kyoto Encyclopedia of Genes and Genomes analyses (KEGG)<sup>29–31</sup>, and Gene Set Enrichment Analysis (GSEA)<sup>32</sup>. The “clusterProfiler” package facilitated automated GO and KEGG term analysis processes<sup>33</sup>. Patients with CCa were divided into two groups, low and high expression, using the median expression level of F2RL1. The analysis was conducted using GSEA (v4.2.3), with a gene set range of 5 to 5000. Statistical significance was determined by a *P*-value of less than 0.05 and FDR less than 0.25<sup>34</sup>.

### Immune-related analysis of F2RL1

We utilized the ssGSEA algorithm from the R package GSVA [version 1.46.0] to compute immune infiltration based on markers for 24 immune cells corresponding to the cloud data from TIMER2.0 (<http://timer.cistrom>

e.org)<sup>35</sup>. Spearman analysis assessed correlations between F2RL1 expression, immune cells, and ICB markers like PDCD1 (PD-1), CD274 (PD-L1), etc. Correlation visualization was achieved by employing the “ggplot2” and “pheatmap” packages. The Wilcoxon rank-sum test evaluated immune infiltrating cells enrichment in CCa patients with high versus low F2RL1 expression.

### Collection of cervical scrapings and serum

Cervical scrapings were collected and then placed into specialized containers for HPV and TCT testing. Participants were classified into distinct groups (10–15 specimens per group) based on the test outcomes: high-risk HPV infection (HPV16, 18+), ASCAS, CIN-I\CIN-II\CIN-III, and precancerous groups. The control group consisted of cervical scrapings obtained from healthy women. All participants provided informed consent for the collection of cervical scrapings and subsequent analysis. The study was conducted in accordance with the Declaration of Helsinki, and the protocol was approved by the Ethics Committee of Shandong Provincial Third Hospital (NO. KYLL-2021065).

### RT-qPCR

In this study, mRNA extraction from cervical scrapings was conducted using Total RNA Extraction Reagent (same as Trizol) (Yeasen, 10606ES60, Shanghai, China). Reverse transcription was conducted in manufacturer for the Strand cDNA Synthesis Kit (Yeasen, 11139ES60, Shanghai, China). Q-PCR experiments were performed on an Applied Biosystems 7500 (Applied Biosystems, USA) using PCR SYBR Green Master Mix (Yeasen, 11184ES25, Shanghai, China). The primer list is as follows: Homo- $\beta$ -actin-250 R: 5'-CTCCTTAATGTCACGCA CGAT-3'; Homo-B-actin-250 F: 5'-CATGTACGTTGCTATCCAGGC-3'; Homo-F2RL1-121F: 5'-GTGTTTGT GGTGGGTTTGCC-3'; Homo-F2RL1-121R: 5'-CAGAGAGGAGGTCAAGCCAAG-3'.

### Western blot

Fifteen micrograms of soluble proteins were loaded onto per lane of a 20% Pre-made BIS-Tris Gel (Thermo). The proteins were separated through electrophoresis and then transferred onto polyvinylidene difluoride membranes. These membranes were then treated with primary antibodies, such as anti-F2RL1 (1:500; Abcam) and anti-Tubulin (1:10,000; Abcam), and subsequently with secondary HRP antibodies (1:20,000; Thermo). Protein levels were quantified using a Bio-Rad imaging densitometer. The experiment was independently replicated three times.

### ELISA

Serum levels of F2RL1 were measured in each group using ELISA with a Human F2RL1 Assay Kit (LSM Bio) following the manufacturer's instructions. Absorbance was measured using a TECAN GENios Plus at 450 nm and repeated three times.

### Statistical analysis

In SPSS 23.0 software, we examined the levels of F2RL1 in both normal and CCa tissues using Kruskal-Wallis test. We also examined the connection between F2RL1 expression and clinicopathological factors by utilizing the chi-square test and multivariate COX regression analyses. Any results showing a *P*-value below 0.05 were deemed statistically significant.

## Results

### Differential expression of F2RL1 in CCa and normal tissues

To investigate potential disparities in F2RL1 expression between CCa tumor tissues and normal tissues, we examined 33 cancer types sourced from The Cancer Genome Atlas (TCGA) and Genotype-Tissue Expression (GTEx). Figure 1A illustrates the expression profile of F2RL1 across pan-cancers from the TCGA + GTEx database, revealing significant differences in 27 cancers, including CCa (Fig. 1B). We then validated the differential expression of F2RL1 in the GSE63678 dataset (Fig. 1C). F2RL1 was prominently located on the right side of the volcano plot, indicating up-regulation. Moreover, the expression of F2RL1 was significantly different in squamous and adenocarcinoma subtypes (Fig. 1D). F2RL1 expression was significantly varied in different pathological stages (Fig. 1E-G). These findings were further confirmed through immunohistochemical analysis of the tissues (Fig. 1H-J).

### Role of F2RL1 in the survival, prognosis, and diagnosis of CCa patients

In this section, we explored the impact of variations in F2RL1 expression levels on the survival, prognosis, and diagnosis of CCa patients. Initially, we constructed a baseline information table using clinical data (Table 1). Survival analysis revealed that patients with CCa exhibiting high F2RL1 expression had lower OS and PFS rates compared to those with low F2RL1 expression (Fig. 2 A-B). Additionally, the analysis of PFI confirmed this trend (Fig. 2C). Notably, survival curves of patients with high and low F2RL1 expression significantly diverged, particularly among clinical stage I patients (Fig. 2D) and those who achieved a complete response (CR) to treatment (Fig. 2E). Additionally, we generated column-line plots depicting OS prognostic outcomes to illustrate the correlation between clinicopathologic variables (e.g., T stage, N stage, M stage) and 1-, 3-, and 5-year survival probabilities (Fig. 2G). Calibration curves for 1-, 3-, and 5-year prognostic predictions demonstrated consistency with our observed results (Fig. 2F), indicating the satisfactory performance of F2RL1-based nomograms. Thus, the differential expression of F2RL1 significantly influenced OS, PFS, PFI, clinical stage I, and CR treatment outcomes among CCa patients, providing pivotal prognostic insights.

COX regression analysis revealed significant differences in F2RL1 expression among N stage categories (N0, N1). Moreover, F2RL1 expression varied across different histologic types, with squamous carcinoma exhibiting

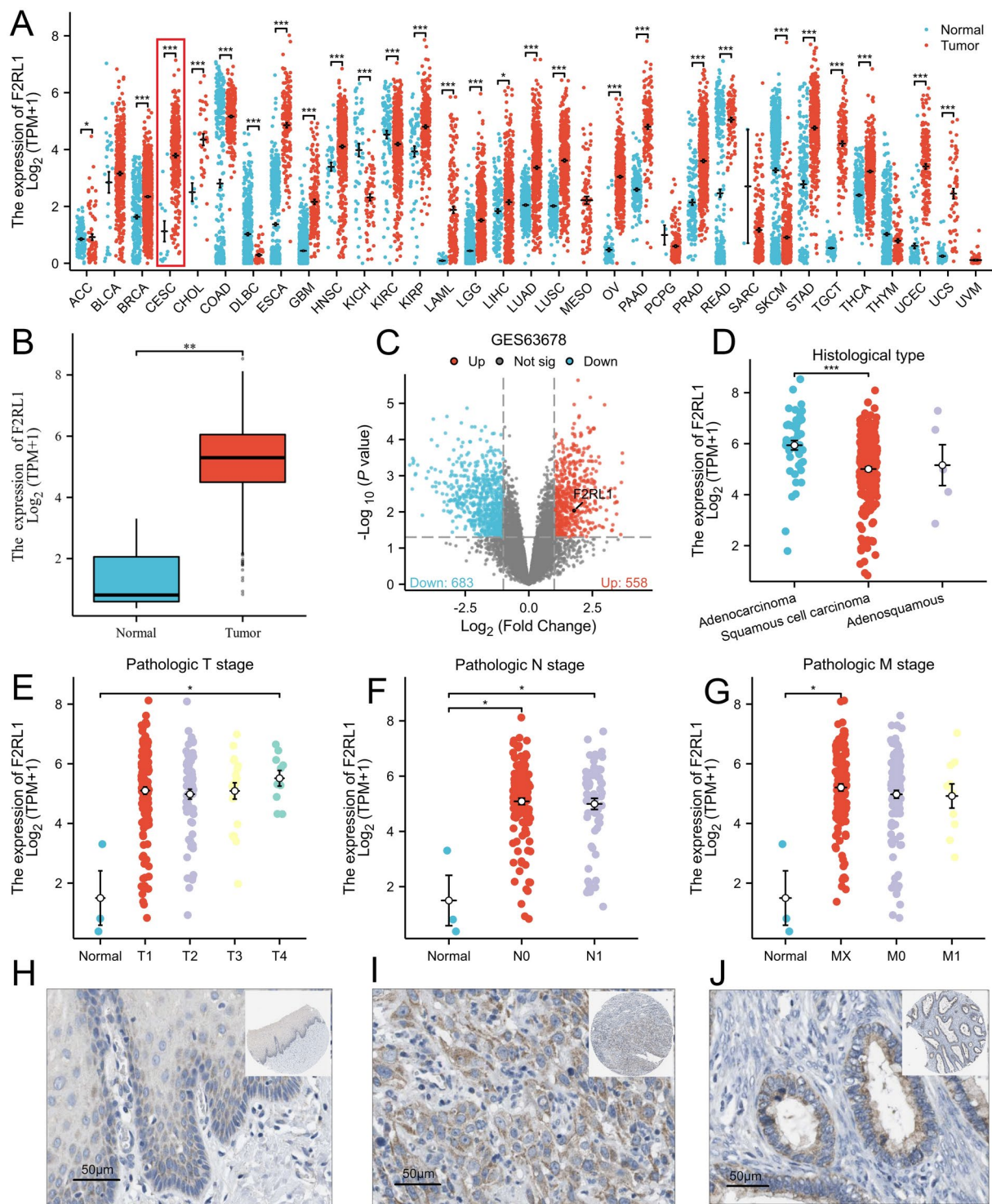


**Fig. 1.** Differential expression of F2RL1 in CCa. **(A)** The expression of F2RL1 in pan-cancer from TCGA + GTEx database. **(B)** F2RL1 mRNA expression shows a marked increase in CCa tissues compared to normal tissues. **(C)** Validation of F2RL1 differential expression in the GES63678 dataset. **(D)** F2RL1 has differentially expressed between squamous and adenocarcinomas in CCa. **(E-G)** The expression of F2RL1 in different pathological stages. **(H-J)** Immunohistochemical staining of the F2RL1 protein in CCa tissue sections. **(H)** normal tissue, **(I)** squamous carcinoma, and **(J)** adenocarcinoma. \*  $p < 0.05$ , \*\*  $p < 0.01$ , \*\*\*  $p < 0.001$ .

Characteristics	Low expression of F2RL1	High expression of F2RL1	P-value
Age, n (%)			0.481
< = 50	91 (29.7%)	97 (31.7%)	
> 50	62 (20.3%)	56 (18.3%)	
n	153	153	
Race, n (%)			0.178
Asian	10 (3.8%)	10 (3.8%)	
Black or African American	20 (7.7%)	11 (4.2%)	
White	98 (37.5%)	112 (42.9%)	
Pathologic T stage, n (%)			0.882
T1	71 (29.2%)	69 (28.4%)	
T2	38 (15.6%)	34 (14%)	
T3	10 (4.1%)	11 (4.5%)	
T4	4 (1.6%)	6 (2.5%)	
Pathologic N stage, n (%)			0.359
N0	71 (36.4%)	63 (32.3%)	
N1	28 (14.4%)	33 (16.9%)	
Pathologic M stage, n (%)			0.551
M0	62 (24.2%)	54 (21.1%)	
M1	7 (2.7%)	4 (1.6%)	
MX	63 (24.6%)	66 (25.8%)	
Clinical stage, n (%)			0.958
Stage I	83 (27.8%)	79 (26.4%)	
Stage II	33 (11%)	36 (12%)	
Stage III	22 (7.4%)	24 (8%)	
Stage IV	11 (3.7%)	11 (3.7%)	
Primary therapy outcome, n (%)			0.700
PD	10 (4.6%)	13 (5.9%)	
SD	4 (1.8%)	2 (0.9%)	
PR	3 (1.4%)	5 (2.3%)	
CR	89 (40.6%)	93 (42.5%)	
<b>Histological type, n (%)</b>			<b>0.001</b>
Adenocarcinoma	12 (3.9%)	35 (11.4%)	
Adenosquamous	4 (1.3%)	2 (0.7%)	
Squamous cell carcinoma	137 (44.8%)	116 (37.9%)	
<b>PFI event (Progression-Free Interval), n (%)</b>			<b>0.007</b>
No	127 (41.5%)	107 (35%)	
Yes	26 (8.5%)	46 (15%)	

**Table 1.** The relationship between F2RL1 expression and the clinical characteristics of CCa.

notably higher expression levels compared to adenocarcinoma and adenosquamous carcinoma (Table 2). This trend aligned with immunohistochemistry findings (Fig. 1F-H), indicating F2RL1's potential in distinguishing cervical squamous carcinoma from adenocarcinoma.

Further analysis comparing CCa tissues with normal groups revealed the promising diagnostic value of F2RL1, as evidenced by ROC curves (Fig. 2H), yielding an AUC of 0.966. F2RL1 also demonstrated diagnostic utility across different racial groups (Fig. 2I), with AUCs exceeding 0.6, aligning with the higher CCa morbidity observed in African-American women compared to whites and Asians. Additionally, F2RL1 exhibited diagnostic value in distinguishing cervical squamous carcinoma, adenocarcinoma, and adenosquamous carcinoma (Fig. 2J-K), consistent with the findings of COX regression analysis (Table 2).

#### Relationship between F2RL1 and immune-related genes

In this section, we utilized immune-related genes sourced from the ImmPort database, totaling 457 genes<sup>36,37</sup>. Through Venn overlap analysis, we identified 43 overlapping target genes among differentially expressed mRNAs (DEmRNAs) associated with the prognosis of CCa patients (Fig. 3A). Figure 3B illustrates the co-expression heatmap of these genes. Notably, the top five genes positively correlated with F2RL1 were AREG, LIF, BMP4, SEMA4G, and FGF5, while the top five negatively correlated genes were CXCL13, CCL19, PNOC, GKN1, and NPPC (Fig. 3E). Subsequently, we conducted a protein interaction analysis using the String database and Cytoscape 3.9.1 software, establishing an interaction network between F2RL1 and the 43 overlapping genes

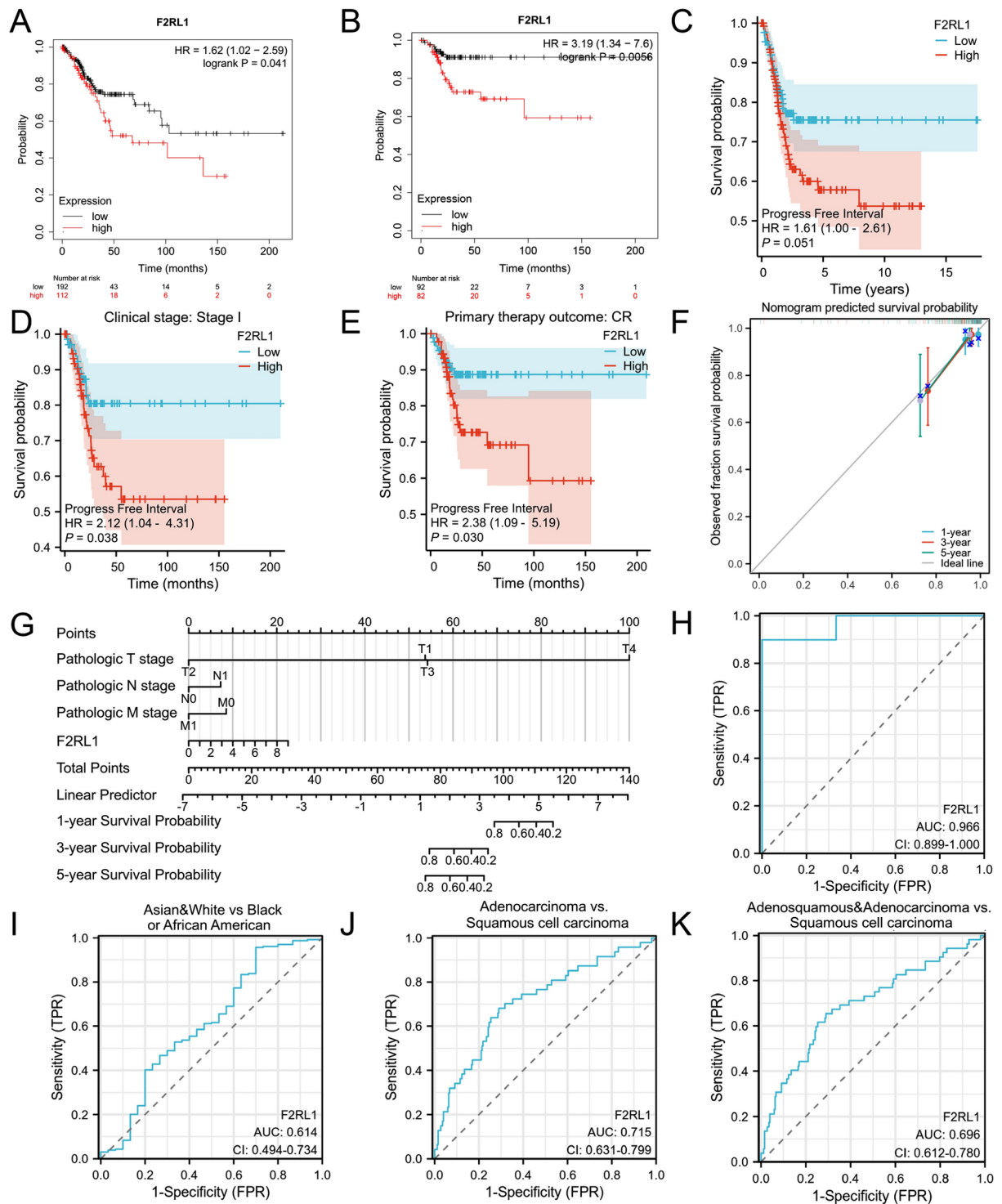


**Fig. 2.** The effect of F2RL1 expression on prognosis and diagnostic value (A-E) Kaplan–Meier analysis of different expression levels of F2RL1. (A) OS, (B) PFS, (C) PFI, (D) Clinical Stage I, (E) Complete responded for primary therapy outcome (F) Nomogram predicted survival probability with calibration curves. (G) The nomogram at 1, 3, and 5 years. (H–K) Diagnostic Value of F2RL1 in CCa. (H) ROC curve demonstrated the diagnostic value of F2RL1 in CCa. (I–K) ROC curve for F2RL1 in different races and pathological types.

(Fig. 3C). Further analysis utilizing different algorithms identified hub genes, with LIF, FGF3, CXCL5, GAST, FGF5, FGF20, FGF19, and CXCL13 being the top-ranked occurrences (Fig. 3D).

Additionally, we conducted a differential gene analysis of immune-related genes, including F2RL1, and visualized the results with a heatmap, indicating positively and negatively correlated genes (Fig. 4A). Functional enrichment analysis using GO revealed associations of F2RL1 with various molecular functions (MF), cellular

Characteristics	Total (n)	OR (95% CI)	P-value
Age(> 60 vs. < 60)	82	1.592 (0.676—3.749)	0.288
Race (Black or African American vs. Asian&White)	80	3.815 (1.271—11.457)	<b>0.017</b>
Pathologic T stage(T3 & T4vs T1 & T2)	79	0.942 (0.414—2.142)	0.887
Pathologic N stage (N1 vs N0)	78	2.337 (1.007—5.425)	<b>0.048</b>
Pathologic M stage(M1 vs M0)	36	2.384 (0.692—8.220)	0.169
Pathologic stage (stage III&IV vs stage I&II)	35	2.267 (0.654—7.860)	0.197
Histological type(Squamous carcinoma vs. Adenocarcinoma& Adenosquamous)	299	3.066 (1.545—6.086)	<b>&lt;0.001</b>
Primary therapy outcome(CR vs. PD&SD&PR)	64	0.101 (0.031—0.336)	<b>&lt;0.001</b>

**Table 2.** One-way COX regression analysis of F2RL1 in CCa.

components (CC), and biological processes (BP). Notably, F2RL1 was implicated in processes such as cilium movement, microtubule bundle formation, and axoneme assembly (BP); as well as cellular components like the apical part of cells, apical plasma membrane, and clusters of actin-based cell projections (CC). Additionally, molecular function analysis revealed F2RL1's involvement in activities such as anion transmembrane transporter, chloride transmembrane transporter, and solute:sodium symporter (MF). Furthermore, KEGG analysis highlighted co-enrichment of F2RL1 and its co-expressed mRNAs in pathways like Neuroactive ligand-receptor interaction, Bile secretion, and Maturity onset diabetes of the young, among others (Fig. 4B-C).

Moreover, we applied the same methodology to analyze the GO and KEGG pathways of the 43 immune-related genes, augmented by Gene Set Enrichment Analysis (GSEA). This comprehensive approach unveiled a myriad of biological processes and pathways intertwined with these genes, including immunoregulatory interactions between lymphoid and non-lymphoid cells, extrafollicular B cell activation by SARS-CoV-2, IL12 pathway, primary immunodeficiency, etc. Notably, we will discuss the negatively associated immunoregulatory interactions between lymphoid and non-lymphoid cells in the following section (Fig. 4D-E).

### Relationship between F2RL1 and immune infiltration

We investigated the relationships between F2RL1 expression and 23 immune cell types, revealing a predominant inverse proportion across the majority of immune cell infiltrates. Particularly striking was the strong inverse proportion observed in TFH and cytotoxic cells (Fig. 5B&C,  $|R| \geq 0.3$ ). Similarly, other immune cell types such as T cells, NK cells, Treg cells, B cells, aDC cells, and DC cells displayed inverse proportion trends (Fig. 5D-I). These findings align with the negatively regulated pathways identified in the third part of the results. Moreover, we analyzed the expression of tumor immune checkpoints in relation to F2RL1 using the same methodology. Remarkably, there was a notable inverse proportion observed with PD-1 (PDCD1), PD-L1 (CD274), CTLA4, TIM3 (HAVCR2), BTLA, LAG3, TIGIT, LILRB2, LILRB4, IDO1, SIGLEC7, and VSIR (Fig. 6A-L).

Furthermore, we conducted a detailed analysis of 24 immune cell types based on differences in F2RL1 expression levels. Figure 7A-K depict the relationships between T cells, CD8 T cells, Treg cells, B cells, NK CD56bright cells, DC cells, aDC cells, iDC cells, Cytotoxic cells, and TFH cells with F2RL1, respectively. In CCa patients, higher F2RL1 expression correlated with diminished concentrations of immune cell subsets compared to those with lower F2RL1 expression.

Finally, we utilized the Kaplan–Meier Plotter (<https://kmplot.com/analysis/>) to perform detailed analyses of survival parameters under various immune cells enrichment or reduction conditions. Our findings revealed notable disparities in survival curves between groups with high and low F2RL1 expression across several immune cell types, including CD4+, CD8+, NK cells, eosinophils, basophils, macrophages, mesenchymal stem cells and mutation high of F2RL1 (Fig. 8A-I). These results suggest that the presence or absence of certain immune cells may impact the survival outcomes in groups with differing levels of F2RL1 expression.

### Experimental validation of F2RL1 expression in early cervical carcinogenesis

In this section, we gathered serum specimens and cervical exfoliated cells, which underwent TCT and HPV PCR testing, for comprehensive analysis. The results of WB assays and RT-qPCR assays revealed significant differences in ASCAS, the high-risk HPV group, CIN-I\II\III, and protocarcinoma groups compared to the control group. Similarly, ELISA assays conducted on patients' plasma yielded analogous findings, with F2RL1 protein concentrations supporting similar conclusions. These findings strongly imply the potential for early-stage cervical cancer diagnosis through the detection of F2RL1 in both serum and cervical samples (Fig. 9A-C).

### Discussion

F2RL1, a transmembrane protein, exhibits expression in various tumors, spanning from breast cancer and hepatocellular carcinoma to ovarian cancer and glioblastoma. Its functionality was mediated through various signaling pathways such as PLC(phospholipase C), intracellular calcium, MAPK(mitogen-activated protein kinase), I-kappaB kinase/NF-kappaB, and Rho<sup>38</sup>. The TCGA database confirmed the varying levels of F2RL1 expression in CCa and normal tissues across pan-cancerous tissues. Positioned within the q13.3 region of chromosome 5, a locus prone to gene disruptions in hairy leukemia, and a recurrent aberration site in malignancies like ovarian and lung cancer<sup>3,39,40</sup>. F2RL1 hinted at the presence of one or more genes

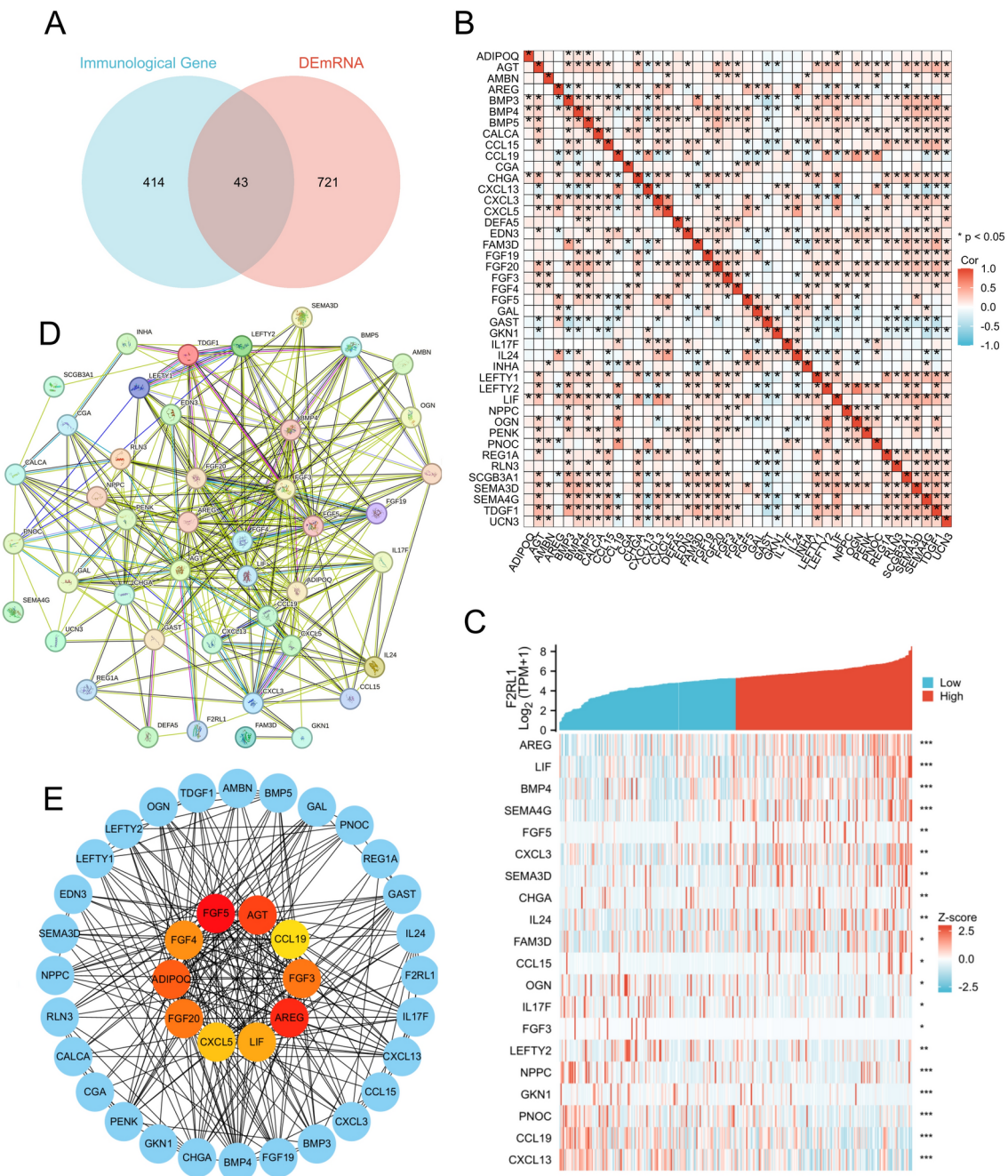


**Fig. 3.** Screening of immunity genes associated with F2RL1 in CCa. (A) A Venn diagram illustrating the overlap between immune-related genes and DEmRNA. Light blue circles denote immune-related genes, while pink circles represent DEmRNA. A total of 43 genes were identified in the screening process. (B) Co-expression heatmap of 43 immune-related genes. (C) The protein–protein interaction network involving 43 immune-related genes (D) Protein interaction network map of 43 genes associated with immune system. By using the Cytoscape plugin, the top ten important nodes are highlighted. (E) Co-expression heatmap of F2RL1 and immune-related genes (with significant differences). \*  $p < 0.05$ , \*\*  $p < 0.01$ , \*\*\*  $p < 0.001$ .

linked to malignant tumorigenesis within this region. Immunohistochemistry results unveiled significantly elevated expression of F2RL1 in different histopathologic subtypes of CCa, including squamous carcinoma, adenocarcinoma, and adenosquamous carcinoma, compared to normal tissues. Notably, the difference in expression between adenocarcinoma and squamous carcinoma was significant, indicating F2RL1's potential to distinguish between these subtypes of uterine cervical cancer. This finding aligned with the results of COX regression analysis. Furthermore, F2RL1 expression exhibited a significant elevation in the cervical *in situ* cancer group relative to the normal group in cervical exfoliated cells, as evidenced by qRT-PCR and WB experiments.

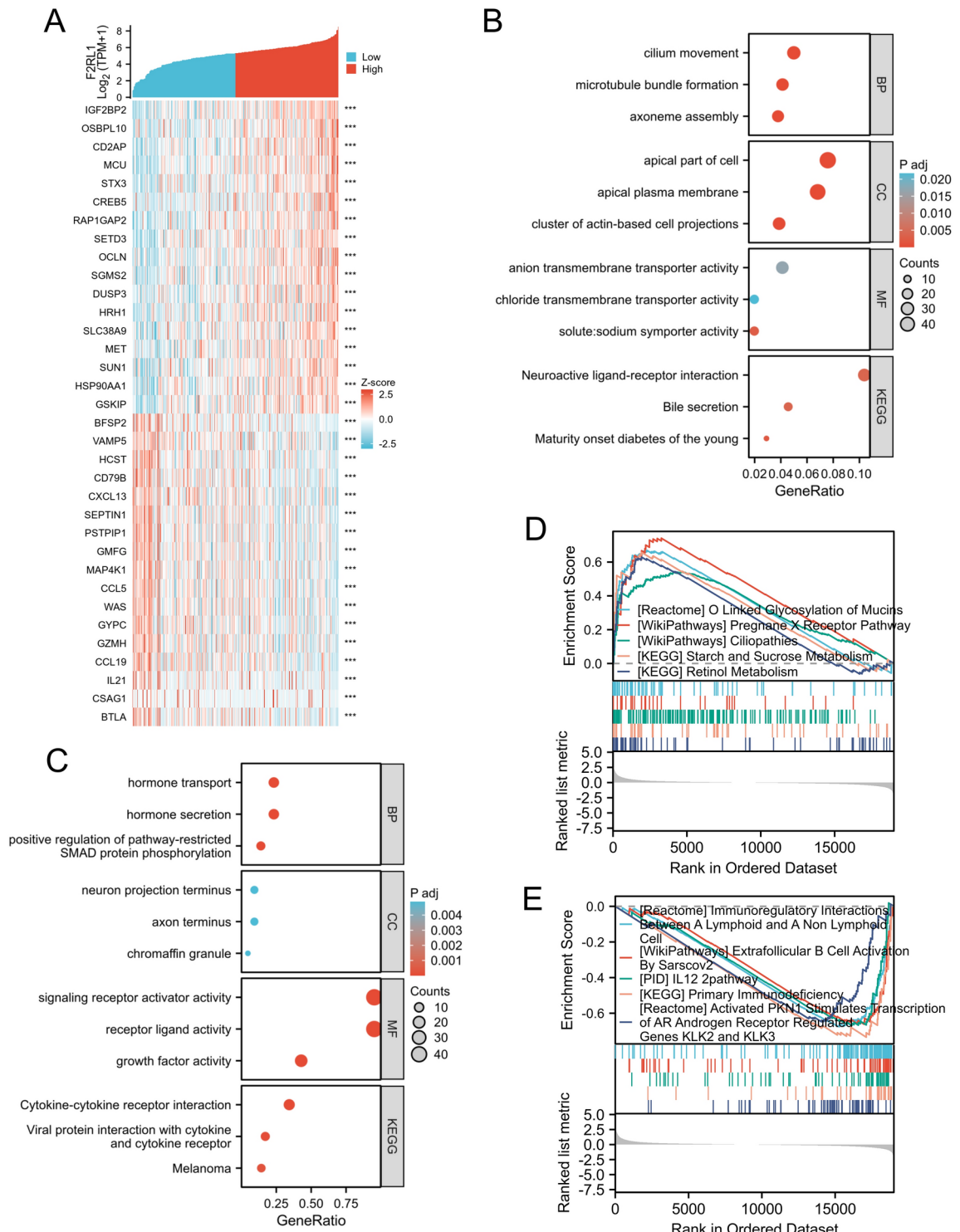


**Fig. 4.** Functional Clustering Analysis of F2RL1-Related DEmRNAs and 43 Immune-Related Genes. **(A)** Heatmap depicting the top 15 DEmRNAs positively and negatively correlated with F2RL1 expression. Genes positively correlated with F2RL1 are highlighted in red, while those showing negative correlations are depicted in blue. **(B)** GO and KEGG analyses of DEmRNAs. **(C)** GO and KEGG analyses of the 43 immune-related genes. **(D,E)** GSEA for the 43 immune-related genes. \*  $p < 0.05$ , \*\*  $p < 0.01$ , \*\*\*  $p < 0.001$ .

Survival analysis revealed that CCa patients with high F2RL1 expression had lower OS, PFS and PFI compared to those with low F2RL1 expression. There was a significant difference in the survival curves for F2RL1 expression between clinical stage I patients and patients in complete remission after treatment. COX regression analysis indicated a significant difference in F2RL1 expression based on the N stage (N0, N1).

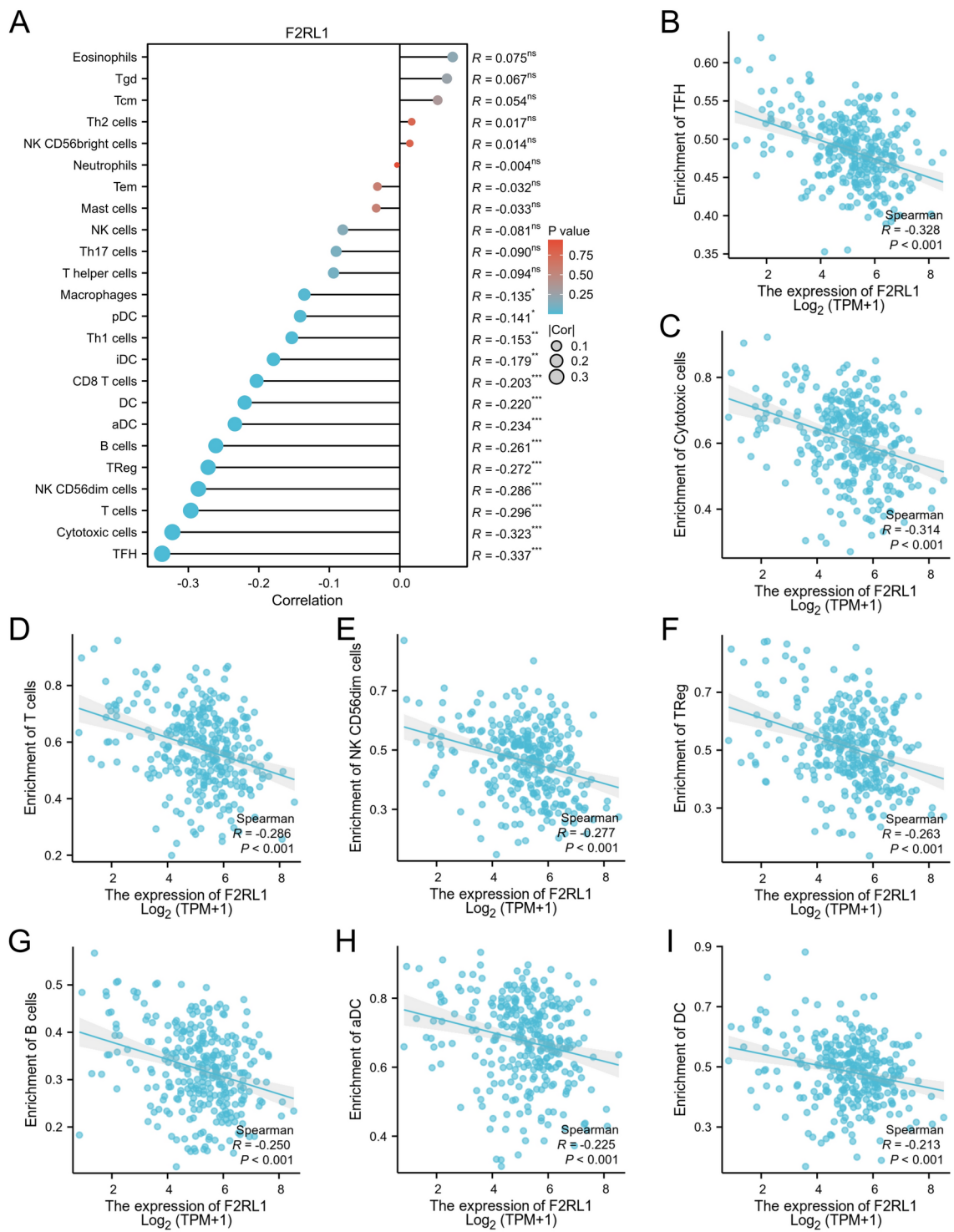


**Fig. 5.** F2RL1 Expression and Tumor Immunity. (A) The bar graph illustrates the correlation between 24 immune cells and F2RL1 expression. Notably, F2RL1 expression displayed a negative correlation with (B) TFH cells, (C) cytotoxic cells, (D) T cells, (E) NK cells, (F) Treg cells, (G) B cells, (H) aDC cells, and (I) DC cells.

Additionally, the ROC curve demonstrated the robust diagnostic value of F2RL1 ( $AUC=0.966$ ). Furthermore, F2RL1 exhibited diagnostic value across different races (White vs. African American) and pathological types (squamous carcinoma, adenocarcinoma). In summation, disparities in F2RL1 expression profoundly influenced the survival trajectories of CCa patients across OS, PFS, PFI, clinical stage I, N stage, and complete remission<sup>41</sup>. We also explored the differential expression of F2RL1 in normal cervical tissue and CCa through bioinformatics analyses and experimental validation. The bioinformatics analysis initially identified significant expression differences of F2RL1. Experimental validation further refined this observation, revealing that the mRNA and

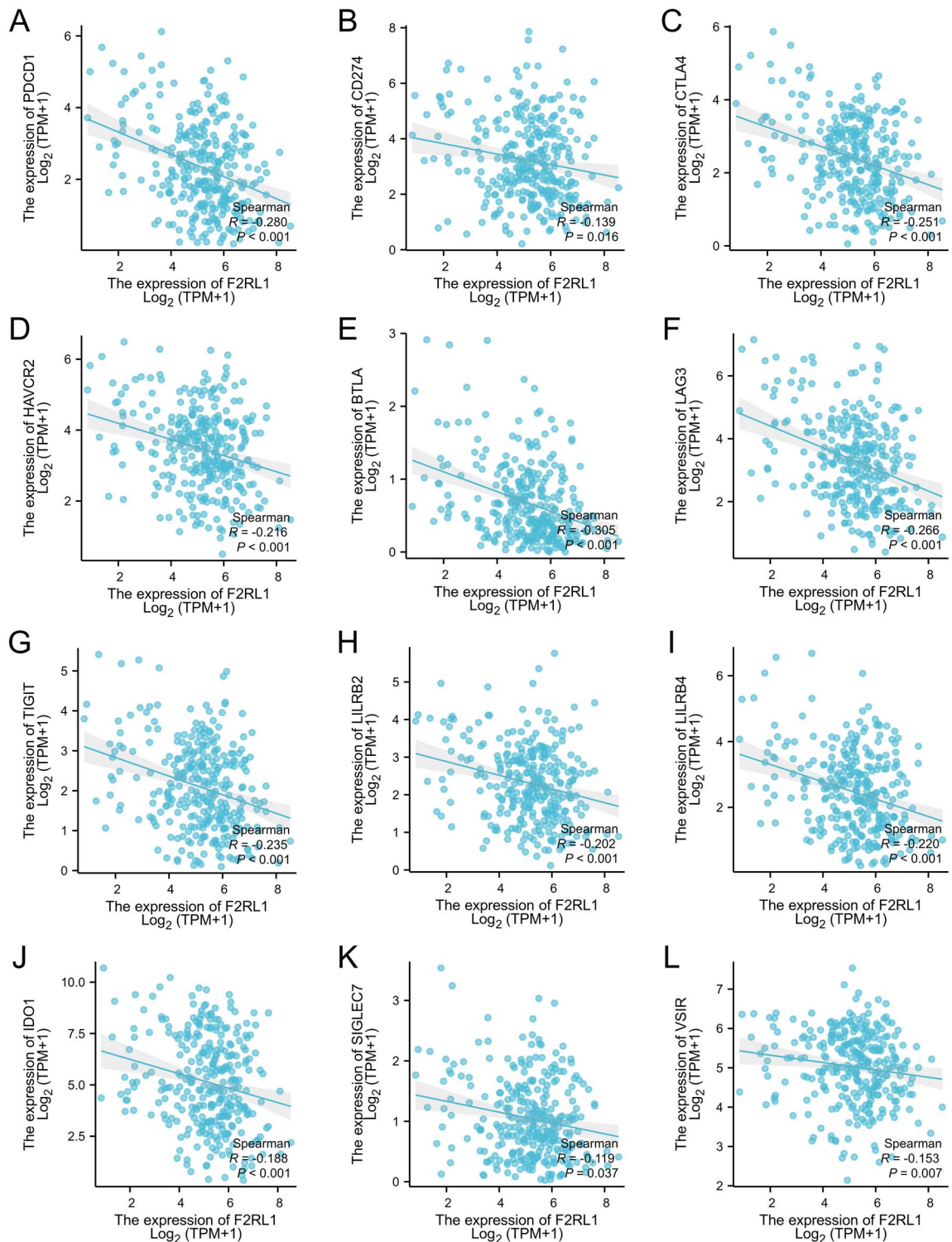


**Fig. 6.** The relationship between immune checkpoints and F2RL1 expression. Significant correlations were observed between F2RL1 and (A) PDCD1(PD-1), (B) CD274(PD-L1), (C) CTLA4, (D) TIM3 (HAVCR2), (E) BTLA, (F) LAG3, (G) TIGIT, (H) LILRB2, (I) LILRB4, (J) IDO1, (K) SIGLEC7, and (L) VSIR.

protein levels of F2RL1 increase rapidly at the ASCUS stage of cervical epithelial cells and reach their peak during HPV infection and CIN I stages. These findings suggest that F2RL1 may serve as an early biomarker for cervical cancer. Based on our data, the cutoff point for F2RL1 expression appears to lie between the stages of HPV infection and CIN I. Given that CCa has a high cure rate when detected and treated early, F2RL1 holds significant potential for clinical application as a predictor for early CCa. Regrettably, no significant “threshold point” for F2RL1 expression was observed in higher-grade epithelial lesions (CIN II, CIN III) or cervical cancer. This lack

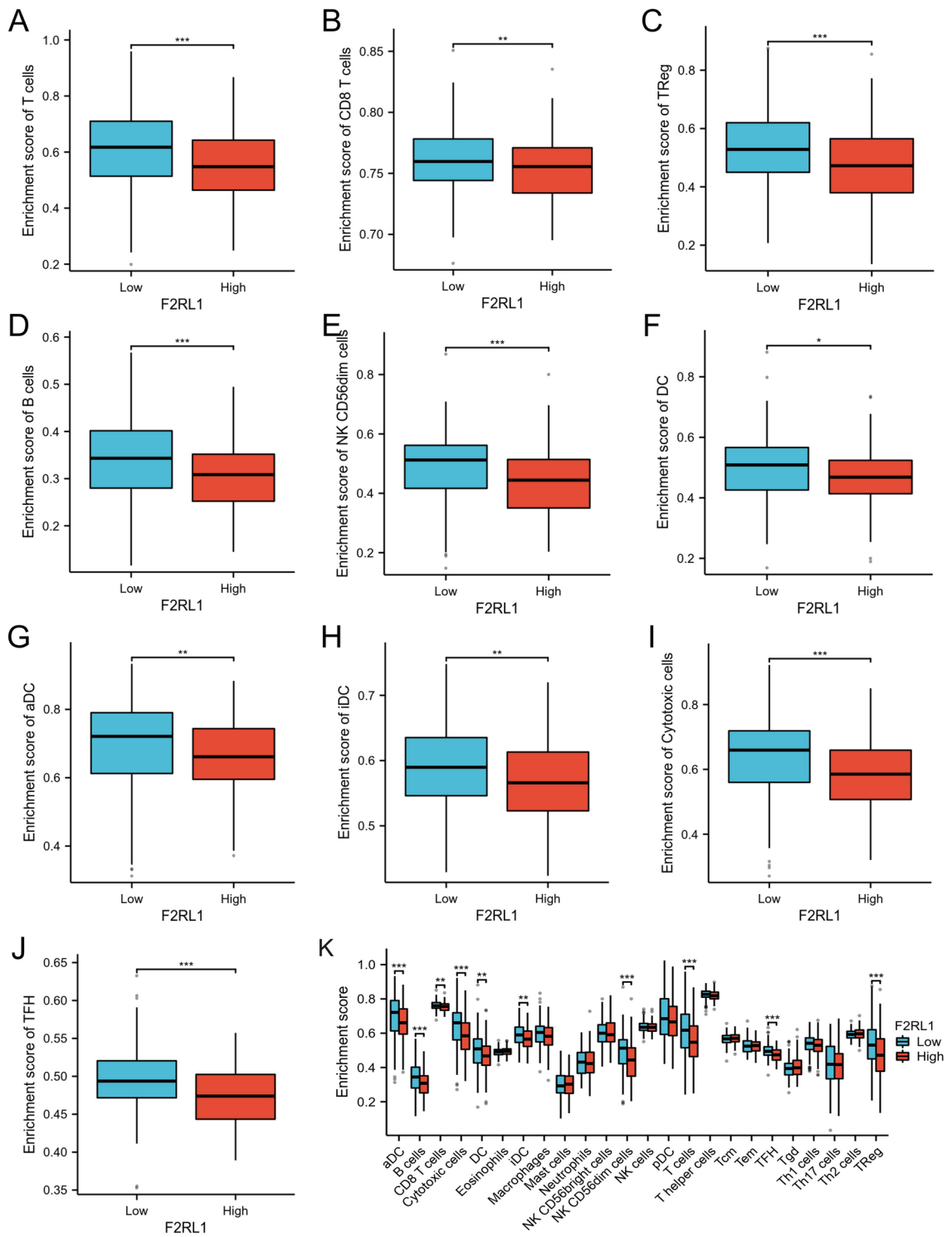


**Fig. 7.** F2RL1 Expression and immune cells enrichment. F2RL1 high expression group had lower enrichment scores of (A) T cells, (B) CD8+ cells, (C) Treg cells, (D) B cells, (E) NK CD56 bright cells, (F) DC cells, (G) aDC cells, (H) iDC cells, (I) Cytotoxic cells, (J) TFH cells, (K) F2RL1 enrichment scores in different immune cells. \*  $p < 0.05$ , \*\*  $p < 0.01$ , \*\*\*  $p < 0.001$ .

of a clear turning point in its expression levels across advanced stages leads us to hypothesize that F2RL1 is more likely a contributing factor to cervical carcinogenesis rather than a consequence of malignant transformation. This suggests that F2RL1 may play a role in the early pathogenesis of CCa, potentially influencing the initiation and progression of precancerous lesions rather than being a byproduct of cancer development. Further research is warranted to elucidate the molecular mechanisms through which F2RL1 contributes to CCa pathogenesis.

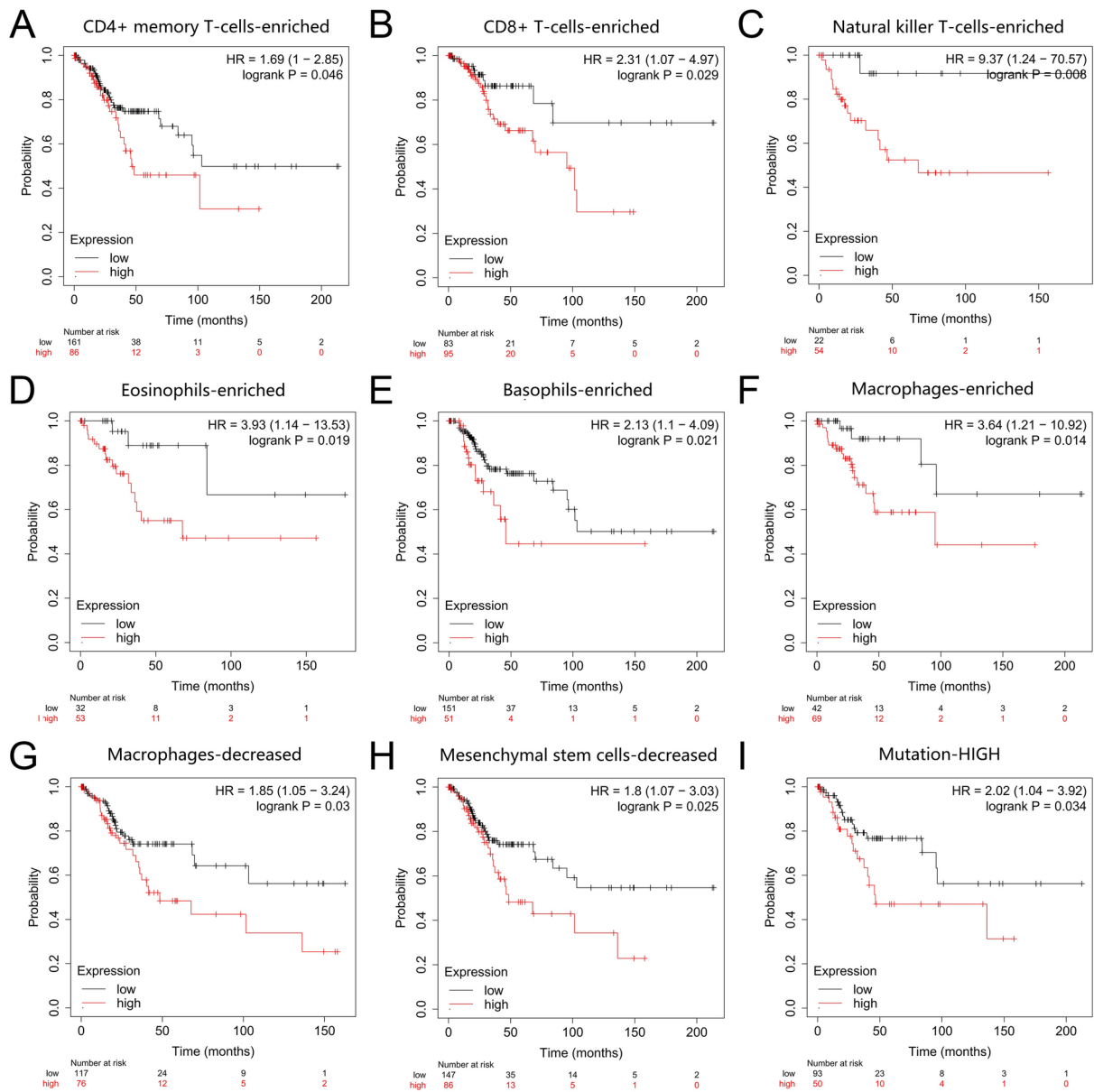


**Fig. 8.** The Kaplan–Meier survival curves comparing the levels of F2RL1 in CCa analyzed based on various immune cell types. Cells enriched: (A) T cells (CD4+), (B) T cells (CD8+), (C) NK cells, (D) Eosinophils, (E) Basophils, (F) Macrophages; Cells decreased: (G) Macrophages, (H) Mesenchymal stem cells. (I) F2RL1 hypermutation.

Regarding endocervical glandular cells, our detection method was based on exfoliated cervical epithelial cells, which precluded differentiation of endometrial glands. However, we conducted a preliminary analysis using the TCGA database and observed that F2RL1 is also highly expressed in endometrial cancer (Fig. 1). This observation provides a foundation for future research into the potential role of F2RL1 in endometrial glandular lesions.

We delved deeper into the genetic landscape associated with F2RL1 expression, meticulously selecting the top 15 genes exhibiting positive and negative correlations. Cell movement plays a crucial role in immune cell function<sup>40,42,43</sup>. Consequently, we retrieved 457 genes from the ImmPort database and intersected them with F2RL1-related genes, resulting in 43 overlapping target genes. Subsequently, GO, KEGG, and GSEA enrichment analyses were performed, revealing negatively correlated immune-regulatory interaction pathways between lymphocytes and non-lymphocytes. F2RL1 orchestrates the recruitment of leukocytes to inflamed sites and stands as the principal PAR receptor, finely tuning eosinophil function, including the secretion of pro-inflammatory cytokines, superoxide generation, and degranulation. During inflammation, in times of inflammation, it plays a key role in enhancing the maturation of dendritic cells, guiding them to lymph nodes, and sparking the activation of T-cells<sup>44</sup>. Nonetheless, this intricate mechanism falters in CCa, hinting at a disruption in F2RL1's

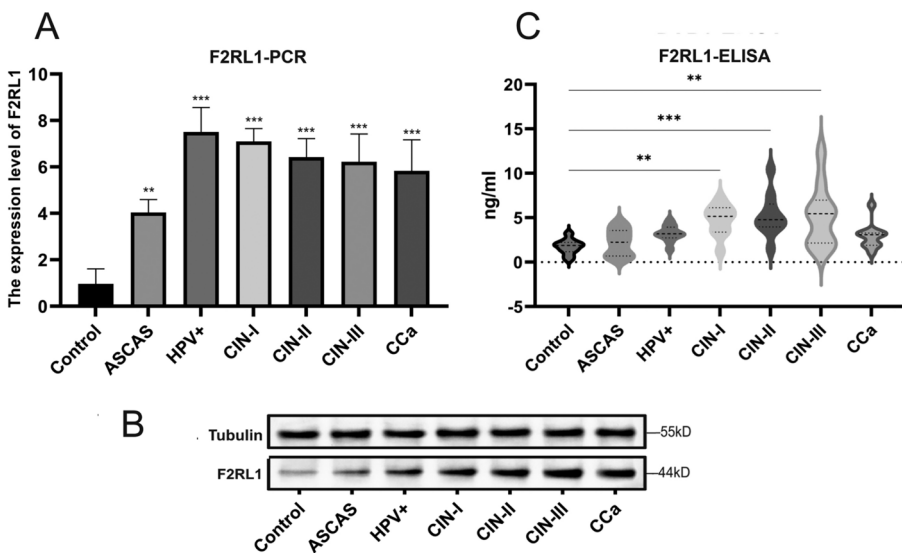


**Fig. 9.** F2RL1 expression in cervical exfoliated cells and serum. (A) RT-PCR assay for detecting F2RL1 mRNA expression in cervical exfoliated cells. (B) Western Blotting for detecting F2RL1 protein expression in cervical exfoliated cells. Original blots are presented in Supplementary Fig. 1. (C) ELISA assay for detecting F2RL1 concentration in serum. \*  $p < 0.05$ , \*\*  $p < 0.01$ , \*\*\*  $p < 0.001$ .

capacity to bolster immune cell enrichment. Immune infiltration emerges as a pivotal mechanism in the body's defense against tumors<sup>45</sup>.

To validate our findings, we assessed the correlation between F2RL1 and individual immune cells, identifying 23 relationships between immune cells and F2RL1 expression. Most infiltrating immune cells exhibited a inverse proportion with F2RL1 expression. Particularly noteworthy were the robust inverse proportion observed with TFH cells and cytotoxic cells ( $|R| \geq 0.3$ ). In a publication in *Nature Immunology*, Di Yu discussed how TFH cells can support the development of tertiary lymphoid structures, boost immune cell presence within tumors, and inhibit tumor progression<sup>46</sup>. Additionally, TFH cells can indirectly boost CD8 + T-cell-mediated anti-tumor immunity through IL-21 secretion. Categorized as tumor-infiltrating lymphocytes (TILs), cytotoxic cells reside within the tumor microenvironment, recognizing antigens on tumor cell surfaces and thwarting tumor growth via the release of cytotoxic molecules such as perforin and granzyme B. If elevated F2RL1 expression impedes tumor infiltration, it could facilitate immune evasion within the tumor milieu. Elevated F2RL1 expression inhibits immune cell infiltration, allowing the tumor to undergo immune escape. Furthermore, in terms of immune checkpoint modulation, consider the example of PD-1. Activated T cells express PD-1, which is encoded by the PDCD1 gene, while tumor cells exhibit overexpression of PD-L1, encoded by the CD274 gene, on their cell membrane. The interaction between PD-1 and PD-L1 inhibits T-cell activation, resulting in cell death and facilitating the evasion of tumor cells from immune surveillance<sup>47</sup>. Tumor immunotherapy using immune checkpoint inhibitors (ICIs) has achieved monumental success and improved the prognosis of cancer patients<sup>48</sup>. The majority of immune checkpoints scrutinized in this investigation exhibited a negative correlation with F2RL1 expression, intimating that F2RL1 might impede immune checkpoints, consequently fostering immune cell activation<sup>49</sup>. This demonstrates the positive and negative roles played by F2RL1 in tumor immunity.

Finally, serum specimens, TCT- and HPV-tested cervical scrapings were collected for analysis, as cervical exfoliated cells and serum are easily accessible specimens for patients. WB assays and RT-qPCR results revealed significant variances in HPV high-risk group, ASCAS, CIN-I/CIN-II/CIN-III, and protocarcinoma groups compared to the control group. ELISA outcomes patient plasma indicated a concentration of F2RL1 protein. This implies the detectability of F2RL1 in serum and pap smears for early CCa diagnosis, potentially positioning F2RL1 as a promising adjunct or substitute to HPV and TCT in early CCa detection.

While our findings may shed light on the connection between F2RL1 and CCa, it's important to acknowledge the limitations that were identified in this research. Firstly, potential sample bias could arise from data sourced directly from public databases. Secondly, to enhance result confidence, expanding the sample size is imperative. Lastly, additional experimental validation is needed to clarify the biological functions of F2RL1 both in *vitro* and in *vivo*.

## Conclusions

In this study, a comprehensive analysis of the role of the F2RL1 gene in CCa was conducted using public databases such as TCGA, Kaplan-Meier Plotter, TIMER, and STRING. Validation was further executed through WB, RT-qPCR, and ELISA techniques. This study unveiled, for the first time, the prognostic and early diagnostic significance of F2RL1 in CCa, alongside its correlation with immune infiltration. The findings strongly suggest that F2RL1 is not only significantly linked to the development of cervical cancer but also has the potential to serve

as a biomarker for predicting the outcome and prognosis of CCa patients. Nevertheless, additional experimental validation is imperative to elucidate F2RL1's biological impacts on CCa and its underlying mechanisms.

## Data availability

The datasets used and/or analyzed during the current study are available from the corresponding author on reasonable request.

Received: 2 July 2024; Accepted: 7 February 2025

Published online: 12 February 2025

## References

1. Denny, L., Kataria, I., Huang, L. & Schmeler, K. M. Cervical cancer kills 300,000 people a year - here's how to speed up its elimination. *Nature* **626**, 30–32. <https://doi.org/10.1038/d41586-024-00241-2> (2024).
2. Alouini, S. & Pichon, C. Therapeutic vaccines for HPV-associated cervical malignancies: A systematic review. *Vaccines (Basel)* <https://doi.org/10.3390/vaccines12040428> (2024).
3. Kim, K. K. et al. Role of trypsin and protease-activated receptor-2 in ovarian cancer. *PLoS One* **15**, e0232253. <https://doi.org/10.1371/journal.pone.0232253> (2020).
4. Stevanović, S. et al. Landscape of immunogenic tumor antigens in successful immunotherapy of virally induced epithelial cancer. *Science* **356**, 200–205. <https://doi.org/10.1126/science.aak9510> (2017).
5. Reinhardt, C. et al. Tissue factor and PAR1 promote microbiota-induced intestinal vascular remodelling. *Nature* **483**, 627–631. <https://doi.org/10.1038/nature10893> (2012).
6. Nag, J. K. et al. Low-density lipoprotein receptor-related protein 6 is a novel coreceptor of protease-activated receptor-2 in the dynamics of cancer-associated  $\beta$ -catenin stabilization. *Oncotarget* **8**, 38650–38667. <https://doi.org/10.18632/oncotarget.16246> (2017).
7. Ossovskaya, V. S. & Bunnett, N. W. Protease-activated receptors: Contribution to physiology and disease. *Physiol. Rev.* **84**, 579–621. <https://doi.org/10.1152/physrev.00028.2003> (2004).
8. Kalogera, S. et al. The activation fragment of PAR2 is elevated in serum from patients with rheumatoid arthritis and reduced in response to anti-IL6R treatment. *Sci. Rep.* **11**, 24285. <https://doi.org/10.1038/s41598-021-03346-0> (2021).
9. Yang, J. et al. Leveraging tumor microenvironment infiltration in pancreatic cancer to identify gene signatures related to prognosis and immunotherapy response. *Cancers (Basel)* <https://doi.org/10.3390/cancers15051442> (2023).
10. Choe, H., Sboner, A., Beltran, H., Nanus, D. & Tagawa, S. T. PO-43 - Differential coagulation factor expression in neuroendocrine prostate cancer (PC), metastatic castrate-resistant PC, and localized prostatic adenocarcinoma. *Thromb. Res.* **140**, S192. <https://doi.org/10.1016/j.thrombres.2016.04.049> (2016).
11. Zhou, M., Li, K. & Luo, K. Q. Shear stress drives the cleavage activation of protease-activated receptor 2 by PRSS3/mesotrypsin to promote invasion and metastasis of circulating lung cancer cells. *Adv. Sci. (Weinh)* **10**, e2301059. <https://doi.org/10.1002/advs.202301059> (2023).
12. Abdel Raheem, H. M., Shehata, H. A., Rashed, L. A. & Saleh, M. A. Decreased level of PAR2 in psoriasis and MF patients receiving phototherapy. *Photodermatol. Photoimmunol. Photomed.* **35**, 282–283. <https://doi.org/10.1111/php.12464> (2019).
13. Li, W. et al. Protease-activated receptor 2 stabilizes Bcl-xL and regulates EGFR-targeted therapy response in colorectal cancer. *Cancer Lett.* **517**, 14–23. <https://doi.org/10.1016/j.canlet.2021.05.040> (2021).
14. Ungefroren, H. et al. Transforming growth factor- $\beta$ 1/Activin receptor-like kinase 5-mediated cell migration is dependent on the protein proteinase-activated receptor 2 but not on proteinase-activated receptor 2-stimulated G(q)-calcium signaling. *Mol. Pharmacol.* **92**, 519–532. <https://doi.org/10.1124/mol.117.109017> (2017).
15. Quan, Q., Zhong, F., Wang, X., Chen, K. & Guo, L. PAR2 inhibition enhanced the sensitivity of colorectal cancer cells to 5-FU and reduced EMT signaling. *Oncol. Res.* **27**, 779–788. <https://doi.org/10.3727/096504018x15442985680348> (2019).
16. Tsai, M. C. et al. The role of protease-activated receptor 2 in hepatocellular carcinoma after hepatectomy. *Medicina (Kaunas)* <https://doi.org/10.3390/medicina57060574> (2021).
17. Xu, P. et al. Melittin inhibits proliferation, metastasis, and invasion of glioma U251 cells by down-regulating F2RL1. *Appl. Biochem. Biotechnol.* <https://doi.org/10.1007/s12010-023-04841-y> (2024).
18. Tang, K. L., Tang, H. Y., Du, Y., Tian, T. & Xiong, S. J. PAR-2 promotes cell proliferation, migration, and invasion through activating PI3K/AKT signaling pathway in oral squamous cell carcinoma. *Biosci. Rep.* <https://doi.org/10.1042/bsr20182476> (2019).
19. Nag, J. K. et al. RNF43 induces the turnover of protease-activated receptor 2 in colon cancer. *Faseb J.* **37**, e22675. <https://doi.org/10.1096/fj.202200858RR> (2023).
20. Ma, J. et al. Bcl-xL mediates interferon-beta secretion by protease-activated receptor 2 deficiency through the mitochondrial permeability transition pore in colorectal cancer metastasis. *Cancer Lett.* **580**, 216483. <https://doi.org/10.1016/j.canlet.2023.216483> (2024).
21. Kawaguchi, M. et al. Protease-activated receptor-2 accelerates intestinal tumor formation through activation of nuclear factor- $\kappa$ B signaling and tumor angiogenesis in Apc(Min/+) mice. *Cancer Sci.* **111**, 1193–1202. <https://doi.org/10.1111/cas.14335> (2020).
22. Müßbach, F. et al. Proteinase-activated receptor 2 (PAR2) in hepatic stellate cells - evidence for a role in hepatocellular carcinoma growth in vivo. *Mol. Cancer* **15**, 54. <https://doi.org/10.1186/s12943-016-0538-y> (2016).
23. Ma, X. B., Xu, Y. Y., Zhu, M. X. & Wang, L. Prognostic signatures based on thirteen immune-related genes in colorectal cancer. *Front. Oncol.* **10**, 591739. <https://doi.org/10.3389/fonc.2020.591739> (2020).
24. He, S. et al. Predictive value of protease-activated receptor-2 (PAR(2)) in cervical cancer metastasis. *J. Cell. Mol. Med.* **25**, 1415–1424. <https://doi.org/10.1111/jcmm.16227> (2021).
25. Shanshan, H. et al. Inhibition of protease-activated receptor-2 induces apoptosis in cervical cancer by inhibiting signal transducer and activator of transcription-3 signaling. *J. Int. Med. Res.* **47**, 1330–1338. <https://doi.org/10.1177/0300060518820440> (2019).
26. Robles, J., Prakash, A., Vizcaíno, J. A. & Casal, J. I. Integrated meta-analysis of colorectal cancer public proteomic datasets for biomarker discovery and validation. *PLoS Comput. Biol.* **20**, e1011828. <https://doi.org/10.1371/journal.pcbi.1011828> (2024).
27. Robin, X. et al. pROC: An open-source package for R and S+ to analyze and compare ROC curves. *BMC Bioinform.* **12**, 77. <https://doi.org/10.1186/1471-2105-12-77> (2011).
28. Dai, Y. et al. An immune-related gene signature for predicting survival and immunotherapy efficacy in hepatocellular carcinoma. *Cancer Immunol. Immunother.* **70**, 967–979. <https://doi.org/10.1007/s00262-020-02743-0> (2021).
29. Kanehisa, M. Toward understanding the origin and evolution of cellular organisms. *Protein Sci.* **28**, 1947–1951. <https://doi.org/10.1002/pro.3715> (2019).
30. Kanehisa, M., Furumichi, M., Sato, Y., Kawashima, M. & Ishiguro-Watanabe, M. KEGG for taxonomy-based analysis of pathways and genomes. *Nucleic Acids Res.* **51**, D587–d592. <https://doi.org/10.1093/nar/gkac963> (2023).
31. Kanehisa, M. & Goto, S. KEGG: Kyoto encyclopedia of genes and genomes. *Nucleic Acids Res.* **28**, 27–30. <https://doi.org/10.1093/nar/28.1.27> (2000).

32. Zhao, W. et al. Comprehensive analysis of COMMD10 as a novel prognostic biomarker for gastric cancer. *PeerJ* **11**, e14645. <https://doi.org/10.7717/peerj.14645> (2023).
33. Yu, G., Wang, L. G., Han, Y. & He, Q. Y. clusterProfiler: An R package for comparing biological themes among gene clusters. *OMICS* **16**, 284–287. <https://doi.org/10.1089/omi.2011.0118> (2012).
34. Hänelmann, S., Castelo, R. & Guinney, J. GSVA: Gene set variation analysis for microarray and RNA-seq data. *BMC Bioinform.* **14**, 7. <https://doi.org/10.1186/1471-2105-14-7> (2013).
35. Bindea, G. et al. Spatiotemporal dynamics of intratumoral immune cells reveal the immune landscape in human cancer. *Immunity* **39**, 782–795. <https://doi.org/10.1016/j.immuni.2013.10.003> (2013).
36. Chaussabel, D. & Baldwin, N. Democratizing systems immunology with modular transcriptional repertoire analyses. *Nat. Rev. Immunol.* **14**, 271–280. <https://doi.org/10.1038/nri3642> (2014).
37. Li, S. et al. Molecular signatures of antibody responses derived from a systems biology study of five human vaccines. *Nat. Immunol.* **15**, 195–204. <https://doi.org/10.1038/ni.2789> (2014).
38. Cheng, R. K. Y. et al. Structural insight into allosteric modulation of protease-activated receptor 2. *Nature* **545**, 112–115. <https://doi.org/10.1038/nature22309> (2017).
39. de Boer, C. J., van Krieken, J. H., Schuuring, E. & Kluin, P. M. Bcl-1/cyclin D1 in malignant lymphoma. *Ann. Oncol.* **8**(Suppl 2), 109–117 (1997).
40. Jiang, Y. et al. PAR2 induces ovarian cancer cell motility by merging three signalling pathways to transactivate EGFR. *Br. J. Pharmacol.* **178**, 913–932. <https://doi.org/10.1111/bph.15332> (2021).
41. Huo, H., Feng, Y. & Tang, Q. Inhibition of proteinase-activated receptor 2 (PAR2) decreased the malignant progression of lung cancer cells and increased the sensitivity to chemotherapy. *Cancer Chemother. Pharmacol.* **93**, 397–410. <https://doi.org/10.1007/s0280-023-04630-8> (2024).
42. Das, K. et al. Protease-activated receptor 2 promotes actomyosin dependent transforming microvesicles generation from human breast cancer. *Mol. Carcinog.* **57**, 1707–1722. <https://doi.org/10.1002/mc.22891> (2018).
43. Zeeh, F. et al. Proteinase-activated receptor 2 promotes TGF- $\beta$ -dependent cell motility in pancreatic cancer cells by sustaining expression of the TGF- $\beta$  type I receptor ALK5. *Oncotarget* **7**, 41095–41109. <https://doi.org/10.18632/oncotarget.9600> (2016).
44. Botham, A. et al. Palmitoylation of human proteinase-activated receptor-2 differentially regulates receptor-triggered ERK1/2 activation, calcium signalling and endocytosis. *Biochem. J.* **438**, 359–367. <https://doi.org/10.1042/bj20101958> (2011).
45. Carvalho, É. et al. Protease-activated receptor 2 (PAR2) upregulates granulocyte colony stimulating factor (G-CSF) expression in breast cancer cells. *Biochem. Biophys. Res. Commun.* **504**, 270–276. <https://doi.org/10.1016/j.bbrc.2018.08.169> (2018).
46. Leong, Y. A. et al. CXCR5(+) follicular cytotoxic T cells control viral infection in B cell follicles. *Nat. Immunol.* **17**, 1187–1196. <https://doi.org/10.1038/ni.3543> (2016).
47. Kelly, P. N. The cancer immunotherapy revolution. *Science* **359**, 1344–1345. <https://doi.org/10.1126/science.359.6382.1344> (2018).
48. Cha, J. H., Chan, L. C., Li, C. W., Hsu, J. L. & Hung, M. C. Mechanisms controlling PD-L1 expression in cancer. *Mol. Cell* **76**, 359–370. <https://doi.org/10.1016/j.molcel.2019.09.030> (2019).
49. Jiang, Y., Zhuo, X., Wu, Y., Fu, X. & Mao, C. PAR2 blockade reverses osimertinib resistance in non-small-cell lung cancer cells via attenuating ERK-mediated EMT and PD-L1 expression. *Biochim. Biophys. Acta Mol. Cell Res.* **1869**, 119144. <https://doi.org/10.1016/j.bbamcr.2021.119144> (2022).

## Acknowledgements

We extend our heartfelt gratitude to all those who contributed to this research. Firstly, we thank Professor Xuewei Zhuang for invaluable guidance and insightful discussions, which greatly shaped our study.

Furthermore, We are indebted to our team for their assistance in experiments and data analysis, without which this research would not have been possible.

Finally, we express our appreciation to the editors and reviewers at PeerJ for their constructive feedback and thorough review process, which significantly improved the quality of our manuscript.

We are grateful for everyone's support!

## Author contributions

Yonggang Dai , Hongya Wang and Xuewei Zhuang designed the study. Chunxiang Li , Shiliang Cheng conducted the statistical analysis. Yonggang Dai , Chunxiang Li and Shiliang Cheng contributed to data analysis and interpretation. Yonggang Dai drafted the manuscript, which was reviewed and revised by Yonggang Dai , Chunxiang Li, Shiliang Cheng , Hongya Wang and Xuewei Zhuang. All authors have approved the submitted version of the article.

## Funding

This work was supported by Shandong Society of Geriatrics 2021 Science and Technology Development Plan(No. LKJGG2021W105).

## Declaration

### Competing interests

The authors declare no competing interests.

### Additional information

**Supplementary Information** The online version contains supplementary material available at <https://doi.org/10.1038/s41598-025-89746-y>.

**Correspondence** and requests for materials should be addressed to X.Z.

**Reprints and permissions information** is available at [www.nature.com/reprints](http://www.nature.com/reprints).

**Publisher's note** Springer Nature remains neutral with regard to jurisdictional claims in published maps and institutional affiliations.

**Open Access** This article is licensed under a Creative Commons Attribution-NonCommercial-NoDerivatives 4.0 International License, which permits any non-commercial use, sharing, distribution and reproduction in any medium or format, as long as you give appropriate credit to the original author(s) and the source, provide a link to the Creative Commons licence, and indicate if you modified the licensed material. You do not have permission under this licence to share adapted material derived from this article or parts of it. The images or other third party material in this article are included in the article's Creative Commons licence, unless indicated otherwise in a credit line to the material. If material is not included in the article's Creative Commons licence and your intended use is not permitted by statutory regulation or exceeds the permitted use, you will need to obtain permission directly from the copyright holder. To view a copy of this licence, visit <http://creativecommons.org/licenses/by-nc-nd/4.0/>.

© The Author(s) 2025